ORNL/TM-6050

Numerical Calculation of Impurity Charge State Distributions

E. C. Crume
D. E. Arnurius

OAK RIDGE NATIONAL LABORATORY
OPERATED BY UNION CARBIDE CORPORATION FOR THE ENERGY RESEARCH AND DEVELOPMENT ADMINISTRATION

BLANK PAGE

Printed in the United States of America. Available from
National Technical Information Service
U.S. Department of Commerce
5285 Port Royal Road, Springfield, Virginia 22161
Price: Printed Copy $[illegible], Microfiche $3.00
$4.50

ORNL/TM-6050

Contract No. W-7405-eng-26

FUSION ENERGY DIVISION

NUMERICAL CALCULATION OF IMPURITY CHARGE STATE DISTRIBUTIONS

E. C. Crume and D. E. Arnurius

Date Published - September 1977

Prepared by the
OAK RIDGE NATIONAL LABORATORY
Oak Ridge, Tennessee 37830
operated by
UNION CARBIDE CORPORATION
for the
ENERGY RESEARCH AND DEVELOPMENT ADMINISTRATION

ABSTRACT

The numerical calculation of impurity charge state distributions using the computer program IMPDYN is discussed. The time-dependent corona atomic physics model used in the calculations is reviewed, and general and specific treatments of electron impact ionization and recombination are referenced. The complete program and two examples relating to tokamak plasmas are given on a microfiche so that a user may verify that his version of the program is working properly. In the discussion of the examples, the corona steady-state approximation is shown to have significant defects when the plasma environment, particularly the electron temperature, is changing rapidly.

CONTENTS

BLANK PAGE

1. INTRODUCTION

It is well known that unwanted ions, called impurities, are found in magnetically confined plasmas created for controlled thermonuclear fusion research. The role of impurities in the transport and in the balance of both particles and energy in one of the most promising types of plasma confinement devices, the tokamak,[1] is a topic of intense and widespread current research, both theoretical and experimental. Knowledge of the ionic state (charge state) of a given impurity, or, more generally, of the distribution of charge states of a given impurity element as a function of position in a plasma is critical to such research and its application. For example, the Coulombic friction among various ions and with the electrons which determines classical (i.e., nonturbulent) particle and heat transport depends on the magnitudes of the charge states of the interacting species.[2] Also, as is well known from atomic physics, the quantity and character of the electromagnetic radiation emitted by ions interacting with electrons depend on the ionic charge, and the amount of such radiation lost from a plasma can be an important part of the plasma energy balance.[3] Tokamak plasmas are considered to be "steady state" from the standpoint of equilibrium and stability, but the density and temperatures of the plasma constituents are functions of position in the plasma. Even this "steady-state" plasma must be created from a neutral gas by ionization, and also during the "steady state" there are more or less significant changes in plasma density and temperature as a function of time.

In order to study the temporal evolution of impurity charge states in such plasmas, we have created the computer program IMPDYN[4] (from IMPurity DYNamics) which can be used either alone with proper input or as a subroutine of another program, such as a tokamak transport code,[5] which supplies the necessary input. The atomic physics model we use is the time-dependent corona model,[6] although the code will trivially generate steady-state corona model (corona equilibrium) ionic distributions. The set of coupled first order differential equations describing the model, the rate equations, is integrated in time using an adaptation of a "stiff" equation solver.[7] The number of possible equations to be

integrated for a given high-Z impurity such as tungsten (atomic number 74 -- therefore 75 equations including the neutral species) may itself be large, and there are usually several impurities present, which may yield a large number of equations even if the impurities have low or intermediate atomic numbers.

Thus, the number of equations to be integrated may be cumbersomely large and their integration excessively time consuming, especially if the rate equation solver is being used as a subroutine of another program which already may require a large amount of computer core and/or computation time. Consequently, we have implemented in IMPDYN a scheme by which the program decides which equations govern the evolution of the species present in significant quantities at a given time and integrates only these equations. Because rarely as many as half the possible ionic states of an impurity are likely present in significant quantities at a given point in a plasma at a given time, and frequently much fewer, this scheme can more than halve computation time. Because the level of significance is in input quantity, the user can decide how detailed (or crude) an analysis is to be made.

In Sect. 2, the corona atomic physics model is briefly reviewed, and the sources of the rate coefficients we have used are noted. The mathematics of solution of the rate equations, the scheme for integrating only the "significant" equations, and the current version of IMPDYN are discussed in Sect. 3. Two examples illustrative of the use of the program, an approach to corona equilibrium and a neutral injection heating experiment in a tokamak, are given in Sect. 4. In Sect. 5 the conclusions are summarized. A complete program listing with numerous comment cards and the two detailed examples are given on the microfiche enclosed in a pocket on the inside back cover of the report.

2. THE CORONA MODEL RATE EQUATIONS

2.1 THE CORONA MODEL

The corona model in both its steady-state and time-dependent forms is discussed in detail by McWhirter,[6] so we only summarize here. The time-dependent corona model was evolved from the steady-state corona model, an atomic model proposed to explain certain spectral features of the solar corona.[8,9] The atomic processes involved are electron collisional ionization, radiative recombination, and excitation and spontaneous decay of excited atomic and ionic states. Jordan[10] has more recently included the additional collisional electronic processes of auto-ionization and dielectronic recombination. For plasmas with electron densities and temperatures in the range of interest,[1] we may decouple the radiation problem (i.e., collisional excitation and spontaneous decay) from the ionic distribution problem and consider only the ground states of the ions (and atoms) involved.[6] (In fact, we will not consider the radiation problem any further here, except to remark that by applying the appropriate coefficients one can determine the radiation from the ionic distributions and the recombination rates calculated by IMPDYN.) The time-dependent corona model was first used to analyze laboratory plasmas by Breton[11] and by Hobbs et al.;[12] the latter workers also coupled the model to a plasma transport model. The steady-state model follows from the time-dependent model by setting all the time derivatives of the ion densities equal to zero, so we treat the steady-state model as a special case.

We may state the assumptions of the time-dependent corona model as follows:

(1) It is assumed that the plasma electron velocity distribution can always be adequately approximated by a Maxwellian distribution of temperature T_e, where T_e may, however, be a function of both time and position within the plasma. This assumption has two aspects. First, thermalization of the distribution following changes in plasma conditions is assumed to occur on a much faster time scale than the time scale of the problem we are considering.[6] Also, perturbations to the

Maxwellian due to electric currents and to magnetic geometry effects[1] are neglected as being of too high an order. No assumptions as to the form of the ion (or atom) velocity distribution need to be made other than that its "temperature" must be low enough ($T_i \lesssim T_e$) that the relative electron-ion (-atom) velocity may be approximated by the electron velocity.

(2) It is assumed that all atomic processes result from two-body collisions between electrons and atoms or ions in their ground states. This is straightforward for collisional ionization and radiative recombination, but any auto-ionization and dielectronic recombination rate coefficients used must be related to ground state populations. There are also other perturbative corrections, which are summarized in Ref. 10.

(3) It is assumed that all atomic radiation emitted escapes entirely from the plasma (the optically thin approximation).

We may then write the differential equation governing the time evolution of the density $n_j(\vec{r}, t)$ of the ground state of an ion of charge j,

$$\frac{dn_j}{dt} = n_e[n_{j-1}S_{j-1} + n_{j+1}\alpha_{j+1} - n_j(S_j + \alpha_j)] , \qquad (1)$$

where $n_e(\vec{r}, t)$ is the electron density. The ionization rate coefficient $S_j(T_e)$ for the ion of charge j is the moment of the product of the ionization cross section $\sigma_i(|\vec{v}|)$ with the relative velocity $|\vec{v}|$, which we here take to be the electron velocity, over the assumed Maxwellian electron distribution

$$S_j(T_e) = \frac{1}{n_e} \int d^3v \sigma_i(|\vec{v}|)|\vec{v}| f_{eo}(T_e) . \qquad (2)$$

The recombination rate coefficient $\alpha_j(T_e)$ is a similar moment of the recombination cross section $\sigma_r(|\vec{v}|)$. We reiterate that auto-ionization, dielectronic recombination, or other effects to be included must have rate coefficients which apply to ground state populations. (Otherwise, obviously, we would have to have an enormously increased number of equations — one for each excited state.) For a given element, there are

$Z + 1$ such coupled equations where j ranges (in integral steps) from $j = 0$ (atoms) to $j = Z$ (fully ionized ion, i.e., the bare nucleus). Although analytic solutions of this set are possible if T_e is constant,[6] such solutions are of limited value for real plasmas, and we are led to numerical solutions such as those accomplished by IMPDYN. If the left-hand sides of the $Z + 1$ equations for an element are set equal to zero, the well-known steady-state corona model solution,

$$\frac{n_j}{n_{j+1}} = \frac{\alpha_{j+1}}{S_j} , \tag{3}$$

is obtained, expressing the balance between ionization and recombination rates.

Before discussing the sources of the ionization and recombination rate coefficients, we draw attention to the fact that equations of the form of Eq. (1) obviously do not account for sources and sinks which may arise from particle transport or externally, such as from wall sources of neutral atoms. To account for particle transport in a simple manner, one can add a term $-n_j/\tau_j$ to Eq. (1) where $\tau_j(\vec{r}, t)$ is an appropriate decay time. If τ_j is positive the term represents a sink; if negative, a source. We have not included such terms in IMPDYN because of its planned use with tokamak transport codes for problems in which the transport occurs on time scales such that alternating computation of atomic physics processes and transport can be made. We also do not include external source terms. Such terms may have arbitrary forms, and, in any event, we would try to treat them on the same time scale as the transport; i.e., we consider only weak external source terms.

2.2 THE RATE COEFFICIENTS

2.2.1 General

The selection of the coefficients to use in the solution of the coupled equations of the form of Eq. (1) is decidedly problem-dependent. It might occur, especially for low atomic number elements, that the

ionization and recombination rate coefficients are known as accurately as the changing electron temperature and density environment in the problem. On the other hand, it is probably more likely, at least for tokamak research, that there are insufficient experimental data and/or theoretical calculations to determine the desired rate coefficients to within a factor of two or more. If the rate coefficients are entirely obtained from theory, it may be that the overall problem is such that some or all of the theoretical calculations may be done at the same time as the solution of the rate equations. However, if the atomic physics aspect of the problem is only part of the calculation — say, for example, if one is including impurity atomic physics in a tokamak discharge simulation — such theoretical calculations may be too cumbersome and/or time consuming to include. It is not our purpose here to assess the merits of rate coefficients from different sources. Our own criterion for most of the calculations that we perform is that the coefficients include as much physics as possible while retaining a calculationally simple form. Because the rate coefficient calculations in IMPDYN are handled in subroutines, the user has the option of providing his own subroutines for that purpose. Besides the references to rate coefficients already listed and those to be given below, we refer the reader to the newsletter *Atomic Data for Fusion*[13] for the most current references and summaries of new results. We now turn to a brief discussion of the rate coefficients included in the subroutines of IMPDYN.

2.2.2. Ionization Rate Coefficients

Wherever possible, for both ionization and recombination rate coefficients we use tabulations such as those of Jordan[14] and Summers[15] for two reasons. First, more physics went into such calculations (e.g., dielectronic recombination and auto-ionization) than can be put into simple expressions such as the ones we give below for use when such tables are not available. Also, on a computer, interpolation within a table is more rapid than evaluation of a complicated expression. However, when such tabulations are not available, and this is generally true for high atomic number impurities such as molybdenum and tungsten,

we use H. J. Kunze's semiempirical expression for the ionization rate coefficient[16] with the numerical coefficient reduced by a factor of two as he later suggested:[17]

$$S_j(T_e) = 3.75 \times 10^{-8} \frac{q_j}{E_j} \left[\left(\ell n \frac{4OT_e}{E_j} \right)^3 + 40 \right]$$

$$\times \frac{T_e^{1/2}}{E_j + 3T_e} \exp(-E_j/T_e) \text{ cm}^3 \text{ s}^{-1} . \quad (4)$$

In Eq. (4), q_j is the number of electrons in the outermost shell of the atom or ion, T_e is the electron temperature of the plasma, and E_j is the ionization energy obtained either experimentally[18] or from the theoretical calculations of Carlson et al.[19] when no experimental values are available. We note that we also use Eq. (4) to fill the uncompleted portions of tabulations such as those referred to above.

There are two exceptions to the above discussion, carbon and oxygen. For these two elements we have used unpublished work by Dory[20] based on the results of Beigman et al.,[21] who give

$$S_j(T_e) = A_j(E_j/T_e)^{1/2}/(E_j/T_e + \chi_j) \text{ cm}^3 \text{ s}^{-1} \quad (5)$$

where the values of A_j and χ_j are given in Table 1.

2.2.3 Recombination Rate Coefficients

The calculation of the dielectronic recombination contribution to the total recombination rate coefficient is generally so complicated that we do not calculate it. Consequently, when tabulations of total recombination rate coefficients are not available, except for the cases of carbon and oxygen, we calculate only the radiative recombination rate with a few minor corrections along the line pursued by Jordan.[10] For radiative recombination from the charge state j we use the expression of Burgess and Seaton,[22]

$$\alpha_{jr}(T_e) = 1.12 \times 10^{-13} j^2 E_{j-1}^{1/2}/T_e \text{ cm}^3 \text{ s}^{-1} . \quad (6)$$

Table 1. Parameters for ionization and recombination rate coefficients of carbon and oxygen

Spectroscopic state	A_j ($\times 10^8$)	χ_j	B_j ($\times 10^{12}$)	ψ_j
CI	13.0	0.36		
CII	3.6	0.40	0.165	0.1
CIII	2.4	0.73	0.287	0.5
CIV	0.83	0.78	0.576	0.87
CV	0.104	0.62	0.73	0.9
CVI	0.037	0.62	0.38	0.64
CVII			0.56	1.0
OI	11.0	0.285		
OII	3.35	0.285	0.088	0.1
OIII	1.42	0.33	0.255	0.15
OIV	0.9	0.38	0.412	0.53
OV	0.43	0.42	0.583	0.75
OVI	0.17	0.44	0.777	0.82
OVII	0.034	0.62	0.925	0.93
OVIII	0.013	0.62	0.46	0.74
OIX			0.65	1.0

To this we add the correction due to Wilson[23] for radiative decay from bound levels above the thermal principal quantum number limit n_t to those below

$$\alpha_{jb}(T_e) = 9.60 \times 10^{-13} j^4 \exp(\chi_{tj}/T_e)/n_{tj} T_e^{3/2} \text{ cm}^3 \text{ s}^{-1} , \quad (7)$$

where Wilson[23,24] gives

$$\chi_{tj} = 1.29 \times 10^{-4} (E_j/T_e)^{1/7} n_e^{2/7} \quad (8)$$

and Griem[25] gives

$$n_{tj} = 1.26 \times 10^2 \left(\frac{j^{12} T_e}{n_e^2 E_H} \right)^{1/17} \exp \left(\frac{4j^2 E_H}{17 n_{tj}^3 T_e} \right) , \qquad (9)$$

where E_H is the ionization energy of the hydrogen atom. Two further corrections by Wilson[23] are included but are generally negligible for tokamak plasmas. The first is for three-body recombination from the continuum,

$$\alpha_{jcb} = 4.45 \times 10^{-29} n_e / (j T_e)^2 \text{ cm}^3 \text{ s}^{-1} , \qquad (10)$$

and the second is for collisional de-excitation from levels above the thermal limit n_{tj},

$$\alpha_{jcc} = 1.48 \times 10^{-26} n_e \exp (\chi_{tj}/T_e)/(j n_{tj} T_e)^2 \text{ cm}^3 \text{ s}^{-1} . \qquad (11)$$

For carbon and oxygen recombination we use the expression

$$\alpha_j(T_e) = B_j (E_j/T_e)^{3/2}/(E_j/T_e + \psi_j) \text{ cm}^3 \text{ s}^{-1} \qquad (12)$$

where Dory's[20] values for B_j and ψ_j are given in Table 1.

BLANK PAGE

3. NUMERICAL SOLUTION OF THE RATE EQUATIONS

3.1 THE NORMALIZED CHARGE STATE DISTRIBUTION VECTOR

It is advantageous to work with the normalized form of Eq. (1), so we define the normalized density or concentration of the (j-1)st charge state of an impurity element as

$$y_j \equiv n_j / \sum_{j=1}^{Z+1} n_i \ , \tag{13}$$

where $1 \le j \le Z + 1$. Thus $j = 1$ corresponds to the neutral atom and $j = Z + 1$ corresponds to the fully ionized ion where Z is the atomic number of the impurity element. The indexing is seen to be different from that in Sect. 2 and has been changed from the more physical notation used there to simplify computer programming. We denote by $y = y(t)$ the complete normalized charge state distribution vector of which $y_j = y_j(t)$ is one component. The normalization of the vector y is expressed in matrix notation as

$$e^T y(t) = 1 \ , \tag{14}$$

where

$$e^T = (1, 1, \ldots, 1) \tag{15}$$

and the superscript T is used to indicate the transpose of a matrix.

The vector y is the solution of an initial value problem associated with a system of n linear ordinary differential equations of the form taken by Eq. (1) upon normalization. We designate the ionization rate coefficient for the ion of charge $j - 1$ by I_j, which corresponds to S_{j-1} of Sect. 2. We designate the recombination rate coefficient for the ion of charge j by R_j, corresponding to α_j of Sect. 2. If we define

$$\beta_j = n_e(R_j y_{j+1} - I_j y_j) \ , \qquad j = 1, 2, \ldots, n - 1 \ , \tag{16a}$$

$$\beta_o = \beta_n = 0 \ , \tag{16b}$$

then y satisfies the linear, homogeneous system of ordinary differential equations

$$y_j' = -\beta_{j-1} + \beta_j , \qquad j = 1, \ldots, n , \tag{17}$$

where the prime indicates a time derivative and time dependence usually will not be indicated explicitly. The initial condition is given at $t = t_s$ and satisfies

$$e^T y(t_s) = 1 , \qquad y(t_s) \geq 0 . \tag{18}$$

Equation (17) may be expressed in vector-matrix notation as

$$y' = n_e A y \tag{19}$$

where A is the tridiagonal matrix

$$A = \begin{bmatrix} -I_1 & R_1 & & & & \\ I_1 & -(I_2 + R_1) & R_2 & & & \\ & I_2 & & & & \\ & & & R_{n-2} & & \\ & & & I_{n-2} & -(I_{n-1} + R_{n-2}) & R_{n-1} \\ & & & & I_{n-1} & -R_{n-1} \end{bmatrix} . \tag{20}$$

Because $e^T A = 0$, zero is an eigenvalue of the matrix A. Moreover, it can be shown that the eigenvalues of A are simple, real, and nonpositive. The system of differential equations that y satisfies is called a stiff system because there are some large magnitude negative eigenvalues of the matrix $n_e A$. If a nonstiff numerical integration procedure (e.g., Runge-Kutta or Adams-Moulton) is used to approximate y, a small step size is required to ensure the stability of the integration method, even when the terms associated with the negatively large eigenvalues have become

relatively insignificant. For this reason, an integration procedure designed for stiff systems[7] is used to approximate the solution y.

It is characteristic of the charge state distribution vector that a significant number, often one-third to one-half, of its components are negligibly small at any given time. However, the components that are negligible vary with time. The computational time required to solve a stiff system as described in Eqs. (19) and (20) is proportional to n, the number of equations in the system. If Eq. (19) can be replaced by a reduced system that adequately describes the significant components of the charge state distribution vector, then a marked saving in computational time can be realized. This approach is discussed in Sect. 3.2.

3.2 A REDUCED CHARGE STATE DISTRIBUTION SYSTEM AND ITS ASSOCIATED ERROR

The elimination of some equations from each end of the homogeneous system of differential equations described in Eq. (19) yields a reduced system with an inhomogeneous term. Let the reduced system comprise equations ℓ through k and define

$$\tilde{y}^T \equiv (y_\ell, y_{\ell+1}, \ldots, y_k) . \tag{21}$$

Then the reduced system may be expressed as

$$\tilde{y}' = n_e \tilde{A} \tilde{y} + b \tag{22}$$

where

$$b^T = (-\beta_{\ell-1}, 0, \ldots, 0, \beta_k) \tag{23}$$

and

$$\tilde{A} = \begin{bmatrix} -I_{\ell} & R_{\ell} & & & \\ I_{\ell} & -(I_{\ell+1} + R_{\ell}) & R_{\ell+1} & & \\ & I_{\ell+1} & & & \\ & & & R_{k-2} & \\ & & & I_{k-2} & -(I_{k-1} + R_{k-2}) \quad R_{k-1} \\ & & & & I_{k-1} \quad -R_{k-1} \end{bmatrix} . \tag{24}$$

An analytical representation for the solution to the inhomogeneous problem of Eq. (22) is given by

$$\tilde{y}(t) = \Phi(t)\Phi^{-1}(\tau)\tilde{y}(\tau) + \int_{\tau}^{t} \Phi(t)\Phi^{-1}(s)b(s)\, ds \ , \tag{25}$$

where

$$\tilde{y}_h(t) \equiv \Phi(t)\Phi^{-1}(\tau)\tilde{y}(\tau) \tag{26}$$

is the solution to the associated homogeneous problem with the same initial condition at $t = \tau$. Moreover, Φ is the matrix solution to the matrix initial value problem

$$\Phi' = n_e\tilde{A}\Phi \ , \quad \Phi(\tau) = I \ , \tag{27}$$

where I is the identity matrix of order $k - \ell + 1$.

Define the vector e_j to be that vector whose jth component is unity, whose other components are zero, and whose dimension is to be inferred from the context, and let

$$E_f \equiv -\int_{\tau}^{t} \beta_{\ell-1}(s)\Phi(t)\Phi^{-1}(s)e_1\, ds \tag{28}$$

and

$$E_b \equiv \int_\tau^t \beta_k(s)\Phi(t)\Phi^{-1}(s)e_{k-\ell+1}\, ds \ . \tag{29}$$

Then

$$\tilde{y}(t) - \tilde{y}_h(t) = E_f(t) + E_b(t) \ . \tag{30}$$

Define the function $[\ \ ]^+$ by

$$[\wedge]^+ = \begin{cases} x \text{ whenever } x \geqslant 0 \\ 0 \text{ otherwise} \end{cases} \ . \tag{31}$$

Let

$$E_f^+(t) = \int_\tau^t [-\beta_{\ell-1}(s)]^+\Phi(t)\Phi^{-1}(s)e_1\, ds \geqslant 0 \ , \tag{32a}$$

$$E_f^-(t) = \int_\tau^t [\beta_{\ell-1}(s)]^+\Phi(t)\Phi^{-1}(s)e_1\, ds \geqslant 0 \ , \tag{32b}$$

$$E_b^+(t) = \int_\tau^t [\beta_k(s)]^+\Phi(t)\Phi^{-1}(s)e_{k-\ell+1}\, ds \geqslant 0 \ , \tag{32c}$$

$$E_b^-(t) = \int_\tau^t [-\beta_k(s)]^+\Phi(t)\Phi^{-1}(s)e_{k-\ell+1}\, ds \geqslant 0 \ . \tag{32d}$$

With these functions, $\tilde{y}$ may be expressed as

$$\tilde{y}(t) = \tilde{y}_h(t) + \left[E_f^+(t) + E_b^+(t)\right] - \left[E_f^-(t) + E_b^-(t)\right] \ . \tag{33}$$

Because

$$[-\beta_{\ell-1}]^+ \leqslant n_e I_{\ell-1} y_{\ell-1} \tag{34a}$$

and

$$[\beta_{\ell-1}]^+ \leq n_e R_{\ell-1} y_\ell \ , \tag{34b}$$

it follows that

$$E_f^+(t) \leq \int_\tau^t n_e I_{\ell-1} y_{\ell-1} \Phi(t)\Phi^{-1}(s) e_1 \, ds \tag{35a}$$

and

$$E_f^-(t) \leq \int_\tau^t n_e R_{\ell-1} y_\ell \Phi(t)\Phi^{-1}(s) e_1 \, ds \ . \tag{35b}$$

Also, the components of $\Phi(t)\Phi^{-1}(s)$ are nonnegative and $e^T\Phi(t) = e^T$ for $t \geq \tau$; consequently

$$\|E_f^+(t)\|_1 \leq \int_\tau^t n_e I_{\ell-1} y_{\ell-1} \, ds \tag{36a}$$

and

$$\|E_f^-(t)\|_1 \leq \int_\tau^t n_e R_{\ell-1} y_\ell \, ds \ , \tag{36b}$$

where $\|v\|_1$ denotes the ℓ_1-norm of the vector $v^T = (v_1, \ldots, v_{k-\ell+1})$. That is,

$$\|v\|_1 = |v_1| + \ldots + |v_{k-\ell+1}| \ . \tag{37}$$

In a similar fashion,

$$\|E_b^+(t)\|_1 \leq \int_\tau^t n_e R_k y_{k+1} \, ds \tag{38a}$$

and

$$\|E_b^-(t)\|_1 \leq \int_\tau^t n_e \bar{I}_k y_k \, ds \ . \tag{38b}$$

The reduced system to be used is not the inhomogeneous system described in Eq. (22), which is exact, but the associated homogeneous system

$$\tilde{y}_h' = n_e \tilde{A} \tilde{y}_h \ , \qquad \tilde{y}_h(\tau) = \tilde{y}(\tau) \ . \tag{39}$$

It follows from Eq. (33) that the approximation $\tilde{y}_h$ is low by at most the vector $E_T^+ + E_D^+$ and high by at most the vector $E_T^- + E_D^- - E_T^+(t)$ is associated with the gain into the reduced system from the equations eliminated at the front (low index equations) and $E_f^-(t)$ is associated with the loss from the reduced system to those same equations. But the magnitude of the gain at the front over the time interval $[\tau, t]$ is bounded by the magnitude of the loss to the front over the same time interval plus the sum of the concentrations discarded by the truncation at time τ. Thus,

$$\|E_f^+(t)\|_1 \leq \|E_f^-(t)\|_1 + \sum_{j=1}^{\ell-1} y_j(\tau) \tag{40}$$

and

$$\|E_f^+(t) + E_b^+(t)\|_1 \leq \|E_f^-(t) + E_b^-(t)\|_1 + \sum_{j=1}^{\ell-1} y_j(\tau) + \sum_{j=k+1}^{n} y_j(\tau) \ . \tag{41}$$

From Eqs. (36b) and (38b) it follows that

$$\|E_f^-(t) + E_b^-(t)\|_1 \leq \int_\tau^t n_e (R_{\ell-1} y_\ell + I_k y_k) \, ds \ . \tag{42}$$

Equations (40) and (41) are used in Sect. 3.4 as the basis for the strategy to alter (add to or delete from) the set of active equations and to monitor the error arising from the use of a truncated set.

3.3 PROPAGATION OF THE CURRENT ERROR

Let us assume that at $t = \tau$ the exact solution of the reduced system is denoted by $y(\tau)$ and that $y(\tau)$ is decomposed into

$$y(\tau) = y_a(\tau) + E^+(\tau) - E^-(\tau) , \tag{43}$$

where

$$E^+(\tau) \geq 0, \; E^-(\tau) \geq 0, \; [E^+(\tau)]^T E^-(\tau) = 0 \tag{44}$$

and $y_a(\tau)$ is the computed approximation to $y(\tau)$. From the linearity of the problem it follows that

$$\Phi(t)\Phi^{-1}(\tau)y(\tau) = \Phi(t)\Phi^{-1}(\tau)y_a(\tau) + \Phi(t)\Phi^{-1}(\tau)E^+(\tau) - \Phi(t)\Phi^{-1}(\tau)E^-(\tau) , \tag{45}$$

where Φ is the matrix solution to the problem described in Eq. (27) with $\ell = 1$ and $k = n$. Because $\Phi(t)\Phi^{-1}(\tau) \geq 0$ and because $e^T\Phi(t)\Phi^{-1}(\tau) = e^T$, it follows that

$$\| \Phi(t)\Phi^{-1}(\tau)E^+(\tau) \|_1 = \| E^+(\tau) \|_1 \tag{46a}$$

and

$$\| \Phi(t)\Phi^{-1}(\tau)E^-(\tau) \|_1 = \| E^-(\tau) \|_1 . \tag{46b}$$

Thus, the ℓ_1-norm of each vector term on the right-hand side of Eq. (45) is constant. The accuracy of most integration procedures is expressed in terms of a local truncation error bound, so it would be beneficial if some cancellation in the vector difference in Eq. (45) occurred with time.

Qualitatively there are two basic types of reduced systems. In the first, the reduced system is such that I_j/R_j is large (small) for all j within the reduced system. In this case the tendency is for the distribution to move toward the higher (lower) charge states. This is also true for the associated error vectors. In the second, the reduced system is

such that $I_j/R_j \geq 1$ for some j and $I_j/R_j \leq 1$ for some j. In this situation there is a tendency for the distribution to move toward or reside mainly in the components j + 1 for which I_j/R_j is near one. Again, the error vectors have the same tendency. In this second type with the central tendency we would expect good cancellation in the vector difference in Eq. (45). In fact, in the case of constant temperature and density the three vector terms on the right-hand side of Eq. (45) become proportional to the equilibrium charge state distribution vector as time increases. Hence, in this case, maximal cancellation occurs.

If $\vec{y}(t_s) = (1, 0, \ldots, 0)$ or $(0, \ldots, 0, 1)$, then a significant number of integration steps are often required with the first type of reduced system. Although some cancellation is to be expected with the first type, its degree is indeterminant.

3.4 A STRATEGY FOR MONITORING THE ERROR AND ALTERING THE SET OF ACTIVE EQUATIONS

The results of Sects. 3.2 and 3.3 need to be combined in order to monitor the error more closely on a time interval (τ, t). We let the set of active equations be equations ℓ through k and in Eq. (43) let the components of $y_a(\tau)$ that correspond to deleted equations be zero. Define $\tilde{E}^+(t)$ to be the vector comprising the ℓ through k components of the vector $\Phi(t)\Phi^{-1}(\tau)E^+(\tau)$ appearing in Eq. (45) and define $\tilde{E}^-(t)$ in the obvious way. Then

$$\|\tilde{E}^+(t)\| \leq \|E^+(\tau)\|_1, \quad \|\tilde{E}^-(\tau)\|_1 \leq \|E^-(\tau)\|_1 . \tag{47}$$

Thus, the representation

$$\tilde{y}(t) = \tilde{y}_h(t) + [\tilde{E}^+(t) + E_f^+(t) + E_b^+(t)] - [\tilde{E}^-(t) + E_f^-(t) + E_b^-(t)] \tag{48}$$

includes the error due to an initial error at time τ, as described in Eq. (43), but with the above alteration as well as the error due to using the reduced system of equations.

With the introduction of zeros into $y_a(\tau)$ it follows that

$$\|E^{+}(\tau)\|_1 = \|\tilde{E}^{+}(\tau)\|_1 + \sum_{j=1}^{\ell-1} y_j(\tau) + \sum_{j=k+1}^{n} y_j(\tau) \tag{49a}$$

and

$$\|E^{-}(\tau)\|_1 = \|\tilde{E}^{-}(\tau)\|_1 \ . \tag{49b}$$

Define

$$L(\tau, t) = \int_{\tau}^{t} n_e(R_{\ell-1} y_\ell + I_k y_k)\, ds \ . \tag{50}$$

Then on the interval $[\tau, t]$,

$$\|\tilde{E}^{+}(t) + E_f^{+}(t) + E_b^{+}(t)\|_1 \leq \|E^{+}(\tau)\|_1 + L(\tau, t) \tag{51a}$$

and

$$\|\tilde{E}^{-}(t) + E_f^{-}(t) + E_b^{-}(t)\|_1 \leq \|\tilde{E}^{-}(\tau)\|_1 + L(\tau, t) \ . \tag{51b}$$

Let us assume that at the initial time $t = t_s$ the initial value is exact. Then on the interval (t_s, t)

$$\|\tilde{E}^{+}(t) + E_f^{+}(t) + E_b^{+}(t)\|_1 \leq L(t_s, t) + p(t) \tag{52a}$$

and

$$\|\tilde{E}^{-}(t) + E_f^{-}(t) + E_b^{-}(t)\|_1 \leq L(t_s, t) \ , \tag{52b}$$

where $p(t)$ is the cumulative sum of the values of the deleted components through time t.

The components of the approximation, $\tilde{y}_h$, may be used in L and p with the result that Eq. (52) remains valid. The functions L and p provide a computationally simple means to monitor the error associated with the current set of active equations and to alter the set of active

equations. In fact, except at points where the set of active equations is altered, the time derivative of the bounds on the right-hand side of Eq. (52) is

$$n_e(R_{\ell-1}y_\ell + I_k y_k) \ . \tag{53}$$

The function L may be effectively restrained by requiring the time derivative in Eq. (53) to be bounded. Indeed, if the value of the expression in Eq. (53) becomes too large, then equations should be added to the back of the current system whenever $I_k y_k \geq R_{\ell-1}y_\ell$ or to the front of the system whenever $R_{\ell-1}y_\ell > I_\nu y_\nu$.

A criterion for deleting equations must take two things into account. First, the proposed new set of active equations must have a sufficiently small value for the time derivative given by Eq. (53). Second, the sum of the components associated with the proposed newly deleted equations must be bounded so that the function p does not become too large.

3.5 COMPUTATIONAL PROGRAMS

A collection of subroutines has been compiled from which it is possible to form two separate computer programs. One program, PROGTI, requires that the temperature and density be constant. Here the suffix (and elsewhere the "argument") TI indicates time independence. The other program, PROGTD, allows the temperature and density functions to be time-dependent. The suffix (and elsewhere "argument") TD indicates time dependence.

Program PROGTI is designed for equilibrium calculations. In this case, the system of linear ordinary differential equations describing the normalized charge state distribution vector

$$y' = n_e A y \ , \quad y(t_s) = y_0 \tag{54}$$

has a constant coefficient matrix $n_e A$. PROGTI may be requested to: (1) determine the equilibrium vector associated with Eq. (53), (NCH.NE.0); (2) approximate the eigenvalues of the coefficient matrix $n_e A$ in Eq. (54), (NROOTS.GT.0); (3) integrate Eq. (54) over the time interval (t_s, t_f)

with y_0 specified in subroutine YINIT; or (4) integrate Eq. (54) until the current $y(x)$ first becomes within EPSCC of the equilibrium vector associated with Eq. (54), where subroutine CONEQU contains the two criteria for measuring closeness.

Fundamentally, the equilibrium vector associated with Eq. (54) is determined from the relationship

$$y_{j+1} = (I_j/R_j)y_j \ . \tag{55}$$

However, measures are followed to exclude the occurrence of machine underflows or overflows and to handle zero values for I and R reasonably. The equilibrium vector is approximated within subroutine EQU.

Program PROGTD is designed only to integrate Eq. (54) over the interval (t_s, t_f) where the temperature and density are time-dependent. Subroutines DENTMP(TD), DTDATA, and DTINIT provide for the definition of the temperature and density profiles.

Subroutine MAIN1(TD) is the basic control routine for program PROGTD; subroutine MAIN1(TI) is the basic control routine for program PROGTI. Subroutine DRIVES controls the numerical integraion of Eq. (54). Logic schematics of these three subroutines are given in the flow charts in Figs. 1, 2, and 3.

The subroutines, including numerous comment cards, are listed on the accompanying microfiche lexicographically except that the block data routines come first. The block data routine BDPARM comes first, followed by the set of block data routines BDEL, ordered according to the atomic number of the associated impurity element. The parameter EL is replaced by the chemical symbol for the element. The data within BDEL is for use with the rate coefficient routines, SVIONZ and SVRECZ, but NZ, the atomic number of the element, is used in several other routines. The block data routine BDPARM contains descriptions of all the control parameters that may be used in the definition of the problem to be solved with the computer program. All input to the program is through the block data routine BDPARM for the program PROGTI. For program PROGTD, the additional data describing the time-dependent temperature and density profiles are found within subroutine DTDATA in data statements.

ORNL DWG FED 77576

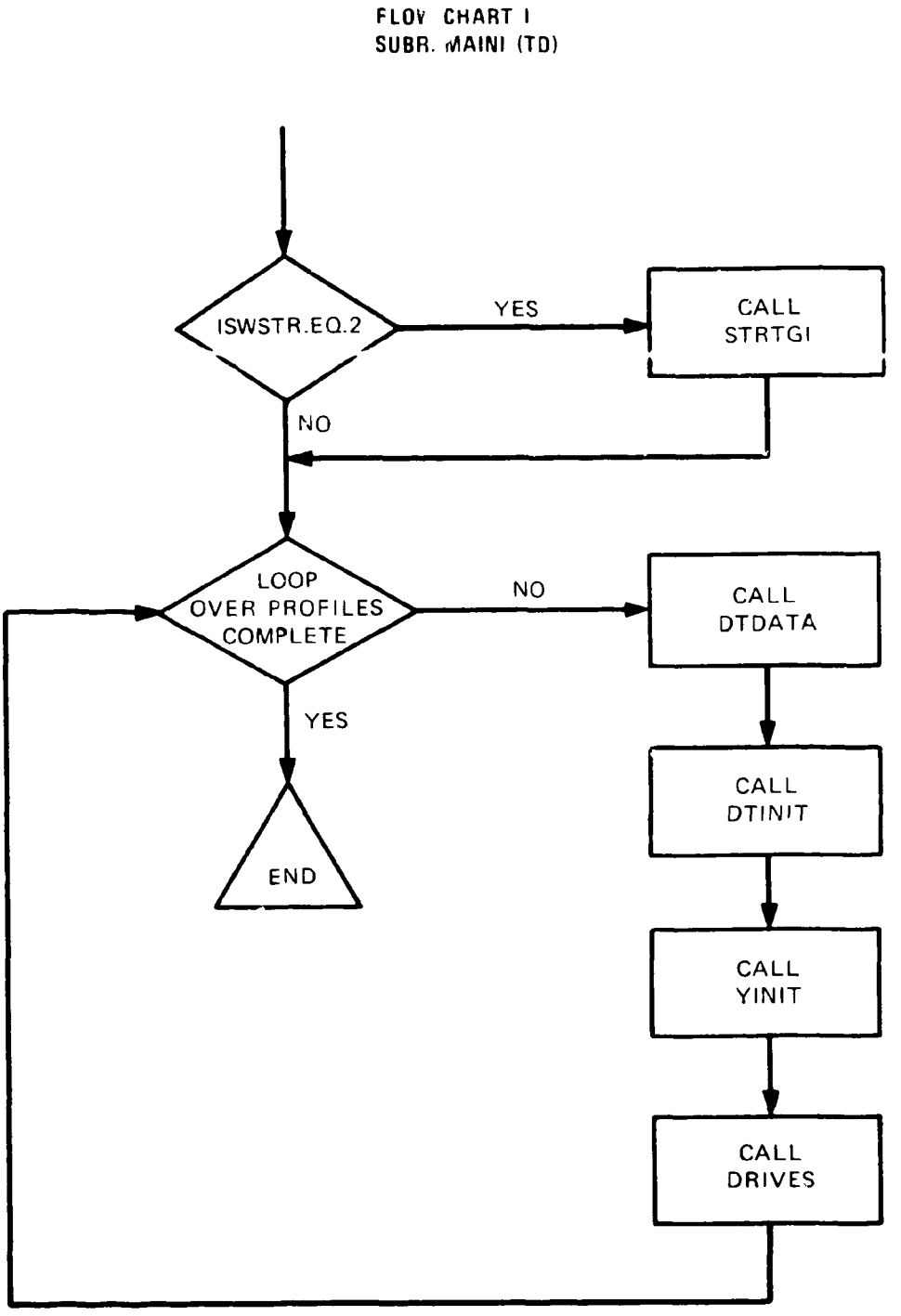

Fig. 1. Logic schematic of IMPDYN program subroutine MAIN1(TD) used when the electron density and temperature are time-dependent.

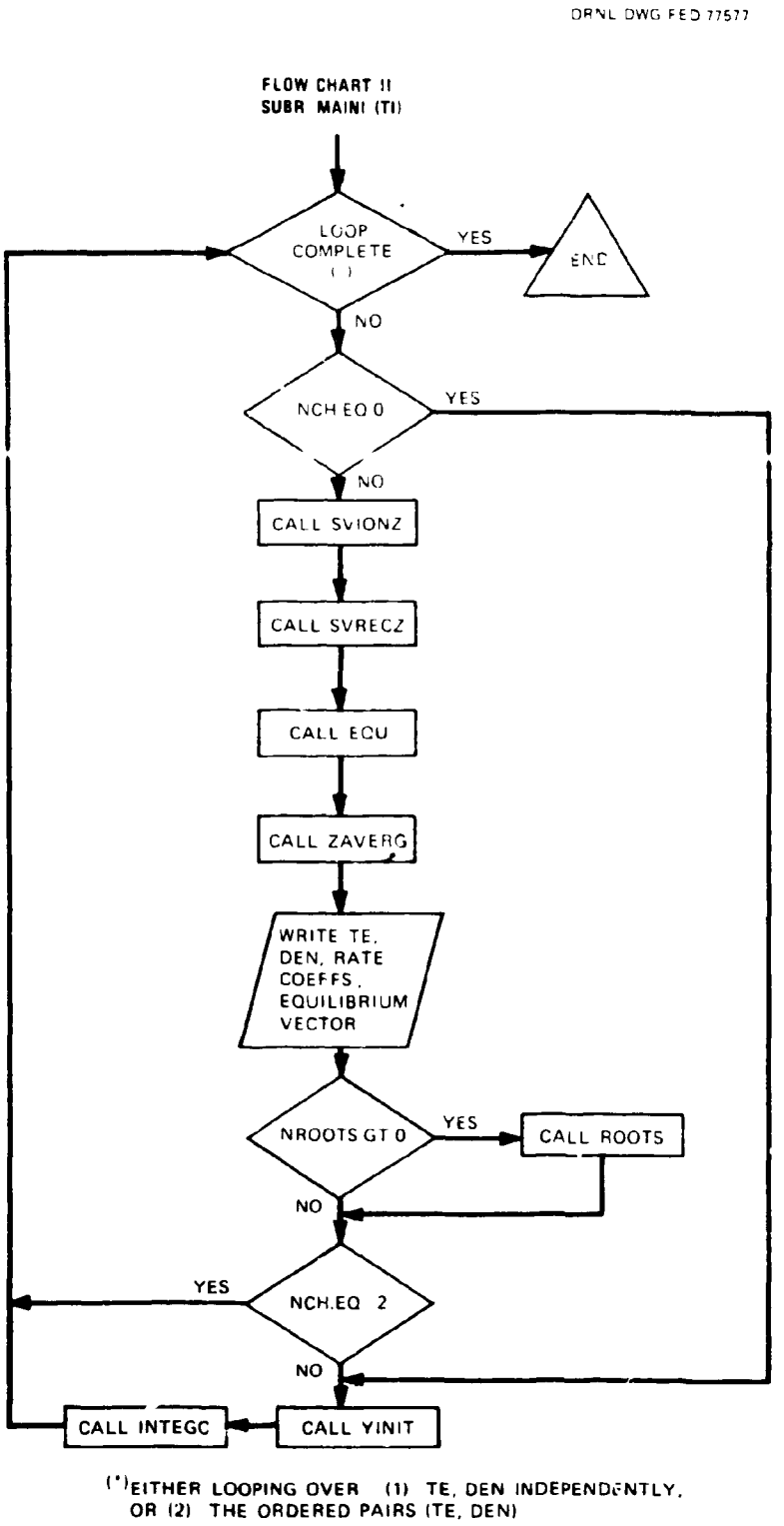

Fig. 2. Logic schematic of IMPDYN program subroutine MAIN1(TI) used when the electron density and temperature are constant (time-independent).

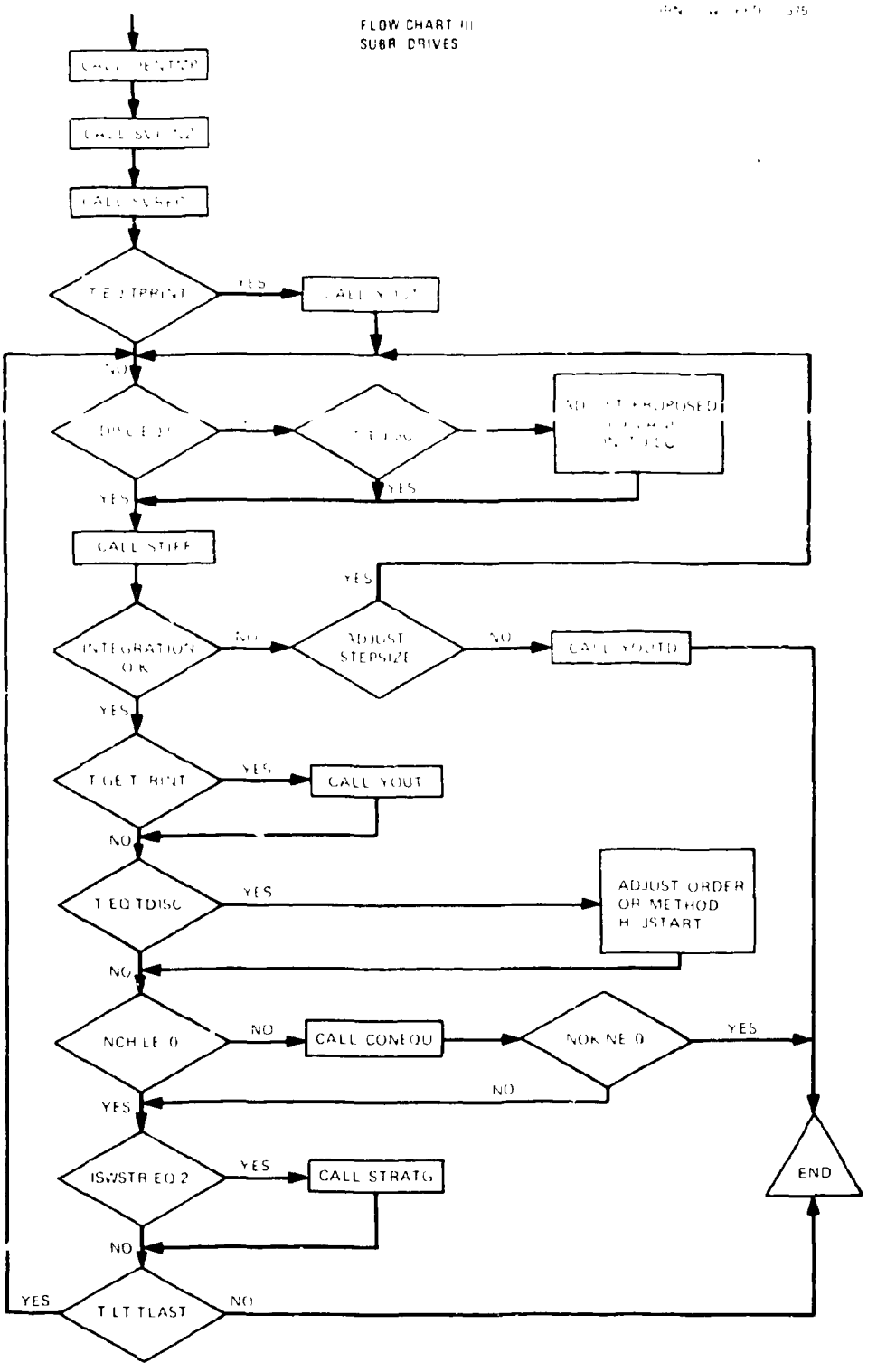

Fig. 3. Logic schematic of IMPDYN program subroutine DRIVES.

Besides describing in the comment cards the kinds of problems the programs PROGTD and PROGTI can solve, the main routine, MAIN, contains two tables that help to reveal the structural organization of the programs and the layout of the labeled commons.

4. EXAMPLES

In this section we discuss the two examples that are included on the microfiche. These examples were chosen to illustrate the use of IMPDYN in its most recent version, to provide benchmarks for checkout of IMPDYN at other installations, and to illustrate some points of physics. Because considerable discussion of input and output for the examples is given on the comment cards associated with the examples on the microfiche, few of the programming details are discussed here and the emphasis is on physics.

4.1 EXAMPLE I: CORONA EQUILIBRIUM

The first example concerns the corona equilibrium charge state distribution of iron in constant plasma conditions where T_e = 500 eV, $n_e = 10^{13}$ cm^{-3}. For the simple general models of ionization and recombination used, in which auto-ionization and dielectronic recombination are neglected, the equilibrium vector is essentially independent of n_e, although there are small corrections which depend on n_e [see Eqs. (7)-(11)]. However, the time required for the charge state vector to approach to within a specified approximation to the equilibrium vector is directly proportional to n_e. This follows directly from Eq. (1), where the time rate of change of a given charge state is seen to be directly proportional to n_e. On page 3 of the Example I part of the microfiche, the normalized equilibrium vector calculated using Eq. (55) [cf. also Eq. (14)] is listed. Only components with concentrations of $\geq 10^{-6}$ are included in the vector. Components with smaller concentrations are neglected and the vector renormalized. This lower bound is set in the data statement card EQU 18 of subroutine EQU. The eigenvalues of $n_e A$ are also listed on page 3. Note that the known zero eigenvalue is not calculated numerically by this single precision program to vanish identically; however, its computed value is about five orders of magnitude smaller than the next larger eigenvalue.

On page 4 of this example, an approach to equilibrium is illustrated. At time t = 0, neutral iron atoms are subjected to the plasma

conditions listed above. Printouts of the distribution have been requested for convergence criteria EPSE = 0.5, 0.1, and 0.01, corresponding to the three values of EPSCC in the block data, card EX.I 50, and at intermediate values controlled by the information on card EX.I 47. The convergence criterion used, NCRIT = 1 (cf. cards BDPARM 35-42, page 2 of program listing), is that the ℓ_1-norm, defined in Eq. (37), of the vector difference between the charge state vector $\tilde{y}_h(t)$ calculated at a given time and the equilibrium vector y_{eq} be less than a prescribed amount. From the listing it is seen that nearly 57 ms are required for $\|\tilde{y}_h - y_{eq}\|_1 < 0.5$. Although this value of EPSE is adequate to get the average charge of the distribution within ~3.5% of its equilibrium value, the concentrations of important states may be incorrect by as much as a factor of two, with possible significant effects on transport and radiation. As would be expected, the lower charge states are overpopulated and the higher states are underpopulated. We also note that 12 equations are current (K - L + 1), those for Fe^{13+} through Fe^{24+}, down from the 14 equations needed at the time t = 0.5 ms of the first printout. The integration step size H is between 2 and 4 ms (H is listed in seconds), up from the initial step size of 5 ns (input quantity H0) needed at the beginning of the integration when the distribution was farthest from equilibrium. It takes nearly 64 ms more to satisfy the next convergence criterion, EPSE = 0.1, at which time the average Z is within less than a percent of its equilibrium value. The dominant charge states are within 10% or so of their equilibrium values at this time. In fact, at t = 110 ms the dominant charge states were within 15% or so, and even at t = 80 ms, within 25% or so. Nevertheless, it is apparent that for this electron density, tens of milliseconds are required for the charge distribution to approach reasonably near to corona equilibrium. These times are on the order of transport times in a tokamak,[24] so the effects of transport should be taken into account, as discussed in Sect. 2. We recall, however, that these times are also inversely proportional to the electron density. For the electron temperature chosen for the example, realistically, the electron density should probably be on the order of a factor of two to three higher.[24]

Consequently, the time estimates should be reduced by the same factor. Such a reduction would still leave the time estimates on the order of transport times, thus leaving open the question of whether corona equilibrium distributions for iron can exist in tokamak plasmas. We address this point further in the next example. We also point out that including auto-ionization and dielectronic recombination in the rate coefficients would change the results for these examples quantitatively (e.g., increase the proportions of the lower charge states) but not qualitatively (i.e., relatively long times are still needed for the approach to corona equilibrium).

4.2 EXAMPLE II: TIME-DEPENDENT T_e AND n_e

In the second example, we study the evolution of the charge state distribution of iron in a plasma environment representative of the central plasma region of the Oak Ridge Tokamak (ORMAK) during electron heating experiments.[24] Laser electron temperature and density data were available for seven times within the discharge period studied, starting at 20 ms, and these are listed at the top of page 4 of the Example II part of the microfiche. In the period before data were available, simple models of the density and temperature evolution were used, and these are listed following the data. As is also indicated on the microfiche, linear interpolation is used to obtain necessary density and temperature information between data points. At each printout time, as chosen in the data statements for TPRNT, DTPRNT, and NPRNT, the distribution of charge states is given, along with other information similar to that given for Example I.

We first note that the time step H in this case, in which the electron temperature is evolving with time, exceeds 1 ms only when the temperature is changing very slowly and never exceeds 2.6 ms. This is in contrast to Example I, in which the temperature was constant and H eventually exceeded 10 ms. In order to best illustrate some of the things that can be learned from this example, we have plotted some of the results of the calculations in Fig. 4. In the upper part of Fig. 4, the evolution of the electron density and temperature is illustrated.

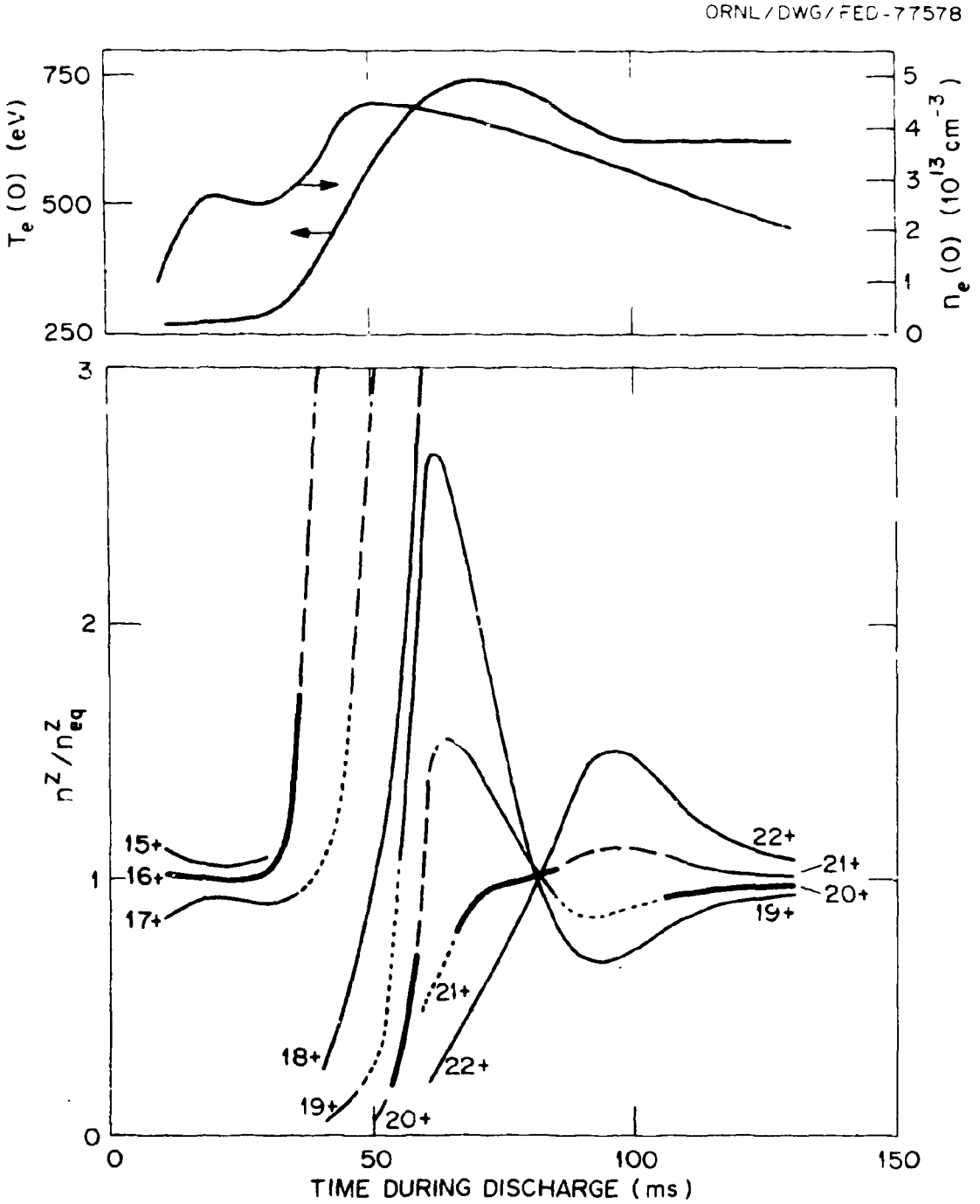

Fig. 4. Ratios of time-dependent to corona steady-state densities of iron ions as functions of time in an ORMAK experiment. In the upper part curves showing the evolution of the central plasma electron density and temperature are given. In the lower part curves are given only for ions with concentrations at least 10% of the total iron density at a given time. The following coding is used for the dominant (greatest fraction of total) ion: (1) heavy line – dominant for both time-dependent and steady-state, (2) broken line – dominant for time-dependent only, (3) dotted line – dominant for steady-state only.

In the lower part of the figure, the evolution of charge states comprising more than 10% of the total impurity at the time of plotting is shown in the following way. The curves plotted are the ratios of the densities (concentrations) calculated using PROGTD, i.e., the concentrations given on the microfiche, to densities (concentrations) for coronal steady state calculated using PROGTI (not given on the microfiche). When a curve is at or near unity, the steady-state approximation is good for that species. Another criterion for the validity of the steady-state approximation is whether it would predict the same dominant (highest concentration) charge state as the time-dependent model. In Fig. 4, the heavy solid line indicates when this is true. When it is not true, the dominant species are indicated as described in the figure caption. As would be expected, the steady-state approximation is worst when the electron temperature is changing relatively rapidly, e.g., in the intervals 30-70 ms and 80-100 ms. Although in the vicinity of 80 ms all the curves are near unity, they have large slopes, so the ratios are changing rapidly. At the end of the calculation, where the temperature has been essentially constant for about 30 ms, the curves are approaching unity. Note that when the temperature is increasing, the time-dependent distribution is weighted toward lower charge states than the equilibrium; when the temperature is decreasing, the opposite is true. Because the excitation rate coefficient for a given species is strongly dependent on the electron temperature,[25] this can have the effect of enhancing the intensity of the radiation emitted when the electron temperature is rising but diminishing it when the temperature is falling. Finally, as was also noted in the discussion of Example I, the atomic physics processes are occurring on time scales comparable to plasma transport time scales, so they must generally be treated time-dependently in transport modeling along with the diffusion processes.

5. SUMMARY AND CONCLUSIONS

In this report, we have discussed a computer program, IMPDYN, that we have found very useful in the study of the evolution of impurities in tokamak plasmas. The program has a number of desirable features, such as minimizing the number of rate equations that need to be solved at any time and allowing any models of ionization and recombination to be used, provided they can be put in a form compatible with the rest of the program. The program has been designed to make this latter step relatively easy by having ionization handled by one subprogram, SVIONZ, and recombination handled by another, SVRECZ, either or both of which may be replaced by equivalent subroutines. The entire program, including two examples which are valuable for checking that the program is working properly, is listed on a microfiche so that the program may be put on any machine. The program is also available from the authors via the National Magnetic Fusion Energy Computer Center.

In the examples we have basically tried to point out that (1) the corona steady-state approximation can be poor when plasma conditions, especially electron temperature, are changing rapidly, and (2) in time-dependent modeling of tokamak discharges there must be interplay between the calculations of the atomic physics processes and the diffusion in order to get them both correct.

REFERENCES

1. L. A. Artsimovich, Nucl. Fusion 12, 215 (1972), H. P. Furth, Nucl. Fusion 15, 487 (1975), S. O. Dean et al., *Status and Objectives of Tokamak Systems for Fusion Research*, WASH-1295, United States Atomic Energy Commission, Washington, D.C. (1974).

2. L. Spitzer, *Physics of Fully Ionized Gases*, 2nd ed., Wiley (Interscience), New York and London, 1962.

3. R. F. Post, J. Nucl. Energy C 3, 273 (1961), Equipe TFR, Nucl. Fusion 15, 1053 (1975).

4. *Thermonuclear Division Annual Progress Report for Period Ending December 31, 1974*, ORNL-5053, p. 38; *Thermonuclear Division Annual Progress Report for Period Ending December 31, 1975*, ORNL-5154, p. 30; and *Fusion Energy Division Annual Progress Report for Period Ending December 31, 1976*, ORNL-52[illegible], p. 135; Oak Ridge National Laboratory, Oak Ridge, Tennessee.

5. J. T. Hogan, Methods in Computational Physics 16, 131 (1976).

6. R.W.P. McWhirter in *Plasma Diagnostic Techniques*, ed. by R. H. Huddlestone and S. L. Leonard, Academic Press, New York, 1965.

7. A. C. Hindmarsh, UCID-30001, Lawrence Livermore Laboratory, Livermore, California (December 1974).

8. R.v.d. Wooley and D.W.N. Stibbs, *The Outer Layers of a Star*, Oxford Univ. Press (Clarendon), London and New York, 1953.

9. G. Elwert, Z. Naturforsch. 7a, 432 (1952).

10. C. Jordan, Mon. Not. R. Astron. Soc. 142, 501 (1969).

11. C. Breton, Euratom Report No. 94, Centre d'Etudes Nucleaires, Fontenay-aux-Roses; *Proc. 5th Intl. Conf. on Ionization Phenomena in Gases*, Vol. 2, p. 2247 (1962).

12. G. D. Hobbs, R.W.P. McWhirter, W. G. Griffin, and T.J.L. Jones, *Proc. 5th Intl. Conf. on Ionization Phenomena in Gases*, Vol. 2, p. 1965 (1962).

13. A bulletin from the Controlled Fusion Atomic Data Center of Oak Ridge National Laboratory and the National Bureau of Standards, edited by C. F. Barnett and W. L. Weise.

14. C. Jordan, Mon. Not. R. Astron. Soc. 148, 17 (1970); private communication, 1975.

15. H. P. Summers, *Tables and Graphs of Collisional Dielectronic Recombination and Ionization Coefficients and Ionization Equilibria of H-like to A-like Ions of Elements*, Appleton Laboratory Internal Memo 367, Culham Laboratory, Abingdon, Oxon (1974).

16. H.-J. Kunze, Phys. Rev. A3, 939 (1971).

17. H.-J. Kunze, Space Science Reviews 13, 565 (1972).

18. W. Finkelnberg and W. Humback, Naturwissenschaften 42, 35 (1955).

19. T. A. Carlson, C. W. Nestor, Jr., N. Wasserman, and J. D. McDowell, Atomic Data 2, 63 (1970).

20. R. A. Dory (Oak Ridge National Laboratory), private communication, 1973.

21. I. G. Beigman et al., Astron. Zh. [Sov. Astron.-AJ] 46, 985 (1969).

22. A. Burgess and M. J. Seaton, Mon. Not. R. Astron. Soc. 127, 355 (1964).

23. R. Wilson, *Plasmas in Space and in the Laboratory*, ESRO SP-20, p. 373, European Space Research Organization, Paris (1967).

24. *Fusion Energy Division Annual Progress Report for Period Ending December 31, 1976*, ORNL-5275, pp. 20 ff., Oak Ridge National Laboratory, Oak Ridge, Tennessee.

25. Equation (23) in R.W.P. McWhirter in *Plasma Diagnostic Techniques*, ed. by R. H. Huddleston and S. L. Leonard, Academic Press, New York, 1965.